JOC The Journal of Organic Chemistry

Article

pubs.acs.org/joc

2,6-Pyridodicarboxamide-Bridged Triptycene Molecular Transmission Devices: Converting Rotation to Rocking Vibration

Guangxia Wang,[†,§,‡] Lishuang Ma,[§] Junfeng Xiang,[†] Ying Wang,[*,§] Xuebo Chen,[*,§] Yanke Che,[*,†] and Hua Jiang[*,†,§]

[†]Beijing National Laboratory for Molecular Sciences, CAS Key Laboratory of Photochemistry, Institute of Chemistry, Chinese Academy of Sciences, Beijing 100190, China

[§]Key Laboratory of Theoretical and Computational Photochemistry, Ministry of Education, Chemistry College, Beijing Normal University, Beijing 100875, China

[‡]University of Chinese Academy of Sciences, Beijing 100049, China

Supporting Information

ABSTRACT: A series of N^2,N^6-bis(triptycene-9-yl)pyridine-2,6-dicarboxamides **1**−**4** were designed and synthesized. Due to rotational constraint of the 2,6-diamidopyridine bridge, the triptycene components in the systems are held together. X-ray structures of **1**−**4** show that the molecules adopt a gear-like geometry in the solid states. DFT (B3LYP/6-31G(d)) calculations predict the gear-like C_2 conformation as global minimum structures for **1** and **2** and suggest that, through a slippage transition process, rotation of one triptycene component would give rise to a rocking vibration of the counter component due to the barrier for rotation of the triptycene components. VT NMR studies on **1**−**4** show that the pair of triptycene components undergo ceaseless slippage at room temperature but nearly freeze at temperatures as low as 183 K. Decreasing the temperature freezes the slippage between triptycene components as well, thus producing the appearance of phase isomers of **3** and **4**. The dynamic features of the studied molecules indicate that this kind of molecule is able to function as a kind of molecular transmission device for transforming the mode of motion from rotation to rocking vibration.

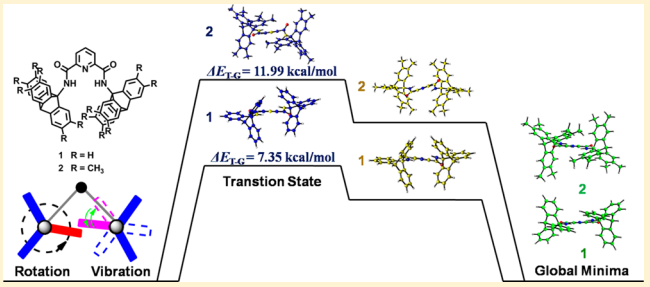

INTRODUCTION

Artificial molecular machines[1,2] have attracted considerable interest due to their attractive potential for construction of ultraminiaturized machines. During the past decades, a variety of molecular machines, such as molecular gears,[3] molecular shuttles,[4] molecular brakes,[5] molecular turnstiles,[6] molecular motors,[7,8] and molecular gyroscopes,[9,10] have been rationally designed and constructed to mimic their macroscopic counterparts. However, few of them adopt mechanical principles from the macroscopic transmission devices used for transforming the mode of movements, although these kinds of machinery components are indispensable in all macroscopic machines.

On the other hand, as a kind of molecular rotary device, molecular gears couple two or more submolecular rotatory components in one molecule, so as to rotate correlatively, to mimic the cogwheeling rotation of macroscopic gears. The three-bladed 9-triptycene (Tp) is well-known as an excellent moiety to build up molecular gears due to its rigid and shape-persistent structure.[1] Since the pioneering studies of Mislow and Iwamura,[11−16] a variety of molecular bevel gear systems based on derivatives of Tp have been designed and synthesized, in which the intermeshed Tp components are coupled by various static atoms or groups, such as CH_2,[11,13,15] O,[12,13,15] S,[15] CHOH,[15] CO,[13a] SiH_2,[15] NH,[14,15] HC═CH,[17] GeCl,[16c,d] and SiF_2[18] (Figure 1). Due to the small axle−axle distance between Tp groups, these molecular bevel gears (Tp_2X or Tp_3X) possess a low energy barrier (1−2 kcal mol^{-1}) for disrotatory cogwheeling (geared rotation) but exhibit a comparatively much higher barrier (>30 kcal mol^{-1}) for correlated conrotations (take place in the process of gear

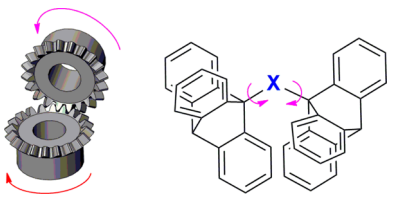

Figure 1. Macroscopic bevel gear and a model for the structure of the reported molecular bevel gears Tp_2X (X = O, CH_2, S, CHOH, CO, SiH_2, NH, HC═CH, or SiF_2. The groups C_3H_2 and GeCl are also used to assemble a cyclic gear with the structure which can be expressed as Tp_3X).

Received: August 1, 2015
Published: October 21, 2015

DOI: 10.1021/acs.joc.5b01778
J. Org. Chem. 2015, 80, 11302−11312

slippage),[11a] indicating that these tightly meshed gears undergo unhindered rotational motions with high gearing fidelity.[19] Accordingly, the ground and the transition states (with C_2 and C_s conformation, Figure S1, Supporting Information (SI)) presented in geared rotation are almost isoenergetic, while the gear-clashed conformation (C_{2v}) has a much higher energy.[11a]

The energy gap between gear-clashed conformation and the ground state, which can be estimated from the activation energy for the gear-slippage process, highly depends on the distance between Tp groups. Longer interaxle distance would typically give rise to a lower barrier. For example, the activation energy for slippage was measured to be 42−43 kcal mol^{-1} in chloro-substituted Tp_2O[12c] (with C(9)−O bond length (d_{C^9-O}) of 1.41−1.42 Å and C(9)−O−C(9′) bond angle ($\varphi_{C^9-O-C^{9'}}$) of 136°), 32−33 kcal mol^{-1} in that of Tp_2CH_2[13c] (with d_{C^9-C} of 1.53−1.57 Å and $\varphi_{C^9-C-C^{9'}}$ of 129°) and ∼21 kcal mol^{-1} in Tp_2SiH_2[15] (with d_{C^9-Si} of 1.86 Å and $\varphi_{C^9-Si-C^{9'}}$ of 129°). Along this line, one may be curious how the dynamic properties of such molecular gears change when the interaxle distance increases further. It has been demonstrated (and is also easy to image) that gearing would lose the efficiency completely when the gears are declutched.[18] But what if the distance keeps increasing but still within a point where the two rotators retain interaction? And is it possible to develop a new molecular device derived from the bevel gears in this state?

Visualization of the dynamic properties of such loosely coupled molecular bevel gears is challenging, considering the uncertainty and diversity in the steric repulsion between Tp groups and the interaxle distance in those unknown systems. One way is to treat the systems as spur gears first, with a presupposition that the Tp rotators are connected with spring-like tension. In this model, given the rigid structure of rotators, the length of the spring under its equilibrium position is very important. A short spring with the length close to that of the radii of Tp rotators would provide a tightly meshed molecular gear, like most of the reported ones,[11−18] with ceaseless dynamic interconvertion between C_2 and C_s states (Figure S1). The C_2 conformation is stabilized by π stacking and orbital interactions, whereas the C_s conformation is stabilized by orbital interactions only. With the increase of the length of spring, the orbital interactions are expected to weaken gradually. To a point, the C_s conformation might not be a local energy minimum anymore. In this process, the gearing fidelity[19] would decrease, which means that C_{2v} (represents gear slippage) and C_{2v}* conformations[20] might be two important transition states in the process of gearing (Figure S1). The maximum axle−axle distance for the C_{2v}* orientation is larger than that of the C_{2v} orientation. Consequently, if the interaxle distance is between the two maximum axle−axle distances for C_{2v} and C_{2v}* orientations, there should be no interaction between two rotators when the gear adopts C_{2v} conformation, which means that there would be a break in the process of rotation transmission from one rotator to the counter one. This is interesting because if the counter rotator could rotate back in every single break with certainty, the rotation of the driving rotator would give rise to a vibration of the counter one. Consequently, the system would not be a molecular gear with low gearing fidelity anymore but a device which could be used to transform the mode of motion. Nevertheless, these speculations are only based on a very simplified mechanical model. Without a concrete molecular model, the transitional states as well as the changes of energy gaps between different states under such conditions compared to that in a tightly meshed mode are difficult to predict, and those will be more complicated when the model is propagated to real molecules under different conditions.

To date, no molecular bevel gears with large interaxle distances are reported. Bryan has previously reported that the incorporation of Tp units into a crown ether created a spur-gear-like structure, but the rotators in it are too far from each other to intermesh.[21] Recently, molecular spur gears with Tp groups bridged with bibenzimidazole were rationally designed and described by Siegel.[20] However, despite considerable energy barriers for gear slippage (calculated to be ∼8 kcal mol^{-1}), the interconversion between phase (*dl* and *meso*) isomers[11a] could not be experimentally observed.

In this contribution, we describe the design, synthesis, X-ray structure, and the dynamic properities of 2,6-pyridinedicarboxamide-bridged Tp derivatives **1**−**4**, which are derived from conventional molecular gears. Due to the appropriate length of the static bridge as well as the large rotation barrier of Tp components, these molecules behave as a kind of molecular transmission device for transforming the mode of motion from rotation of one Tp component to rocking vibration of the counter one. To theoretically determine the most energetically favorable conformational transformation path in the process of intramolecular movement transmission, the minimum energy profiles (MEPs) as a function of the dihedral angle between the planes of one benzene ring in a rotator and the adjacent amide were calculated for **1** and **2** using density functional theory (DFT). Furthermore, dynamic ^{1}H and ^{13}C NMR measurements were also carried out to study the dynamic features of **1**−**4** in solution.

RESULTS AND DISCUSSION

Molecular Design. A molecule that is suitable for studying the rotation of the molecular bevel gear should at least (i) be structurally rigid and shape-persistent under gearing, (ii) have a static group with suitable length, thus keeping the two rotators at an appropriate distance, (iii) maintain the two rotation axles of the rotators coplanar while rotating, and (iv) allow for experimental observation of the intramolecular motions.

Previous studies[22] have shown that 2,6-pyridinedicarboxamides prefer to adopt a stable *cis*-conformation ascribed to the intramolecular hydrogen-bonding between amide and pyridine-N, providing a good motif to construct bent supramolecules such as foldamers. Meanwhile, due to the sp^2 hybridization of the nitrogen atom in amides, the entire 2,6-pyridinedicarboxamide group is planar, which renders rotation of the two rotators around two separate axles within the same plane if this moiety is used as the static in the molecular gears. Furthermore, in contrast to the small axle−axle distance in the molecular bevel gears reported previously,[11−18] the distance between the two amido nitrogens ($d_{N\cdots N}$) in the 2,6-pyridinedicarboxamide group is as large as ca. 4.6 Å, according to the molecular structure, which is about 3.5 fold longer than that of typical double bonds ($d_{C=C}$ = 1.3 Å in ethylene) and about twice the width of a benzene ring (2.4 Å).[23] All these concepts inspired us to design molecules **1** and **2** based on 2,6-pyridinedicarboxamide-bridged Tps, in which the methyl substituents on **2** were designed to increase the size of the gear blade, thus being useful for studying the effect of the blade size of rotators on the dynamic properties.

In conventional Tp-based molecular gears, the subsitituents on the bridgehead carbons were typically designed to produce negligible steric interference in the rotation of rotators.[20,24] In

DOI: 10.1021/acs.joc.5b01778
J. Org. Chem. 2015, 80, 11302−11312

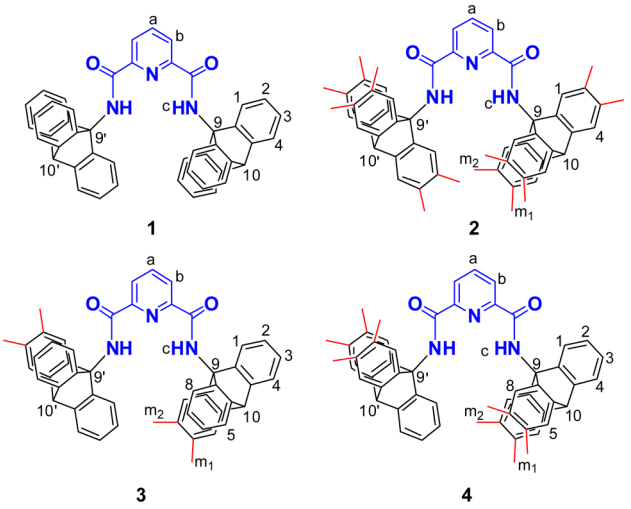

this way, the effect of stereodynamics of the subsitituents themselves on that of gearing could be ignored. This method could simplify the stereochemistry analysis of the gearing behaviors but will give rise to rapid and frictionless rotation of the Tp groups (no matter with or without cogwheel rotation) which are not detectable on the NMR time scale. For the designed molecules, the introduction of an amide would destroy the symmetry of the Tp group and produce an extra rotation energy barrier arising from the steric effect of the carbonyl oxygen atom of the amide, in which the extra rotational barrier might increase the coalescence temperature in dynamic NMR experiments, thus rendering the rotation of Tp to be technically measurable. More importantly, this extra barrier might be able to define an equilibrium position of the Tp components, by which the Tp groups keep a trend to rotate back as long as it deviates from the equilibrium position.

Molecules **3** and **4**, which have two and four methyl subsitituents on each Tp rotator, respectively, and can be regarded as a hybrid of **1** and **2**, were designed for better understanding the relationship between the size of rotators and the dynamics for the studied systems. Besides, it is noteworthy that, different from molecules **1** and **2**, the subsititution of methyl groups on **3** and **4** will break the equivalence of three benzene rings on each Tp group, giving rise to phase isomers.

Synthesis. Synthetic routes for molecular bevel gears **1**–**4** are outlined in Scheme 1. The key issue in these approaches is to obtain the 9-triptycylamine derivatives, that is, the methyl-substituted 9-triptycylamines.

Tp derivatives are generally synthesized by the Diels–Alder reaction from the corresponding anthracenes and benzynes.[25] However, as pointed out by Yamamoto,[26] this method is unfeasible for 9-triptycylamine derivatives because of the presence of undesirable hydroamination of the amine group with benzynes. The preparation was thus initiated with the 9-nitroanthracene or its derivatives. Addition of an excess of benzenediazonium-2-carboxylate in portions to a solution of 9-nitroanthracene while refluxing provides benzyne in situ by thermal decomposition, which then undergoes Diels–Alder reaction to give the 9,10-adduct, 9-nitrotriptycene (**10**), in 46% yield. The low yield is ascribed to the strong electron-withdrawing nitro group, which is not favorable for Diels–Alder addition, thus giving a considerable amount of 1,4-adduct, 11-nitro-5,12-dihydro-5,12-ethenonaphthacene. The multiple methyl-substituted 9-nitrotriptycenes were prepared from the corresponding derivatives of 9-nitroanthracene and

Scheme 1. Synthesis of 2,6-Pyridinedicarboxamide-Bridged Triptycene and Its Derivatives 1–4[a]

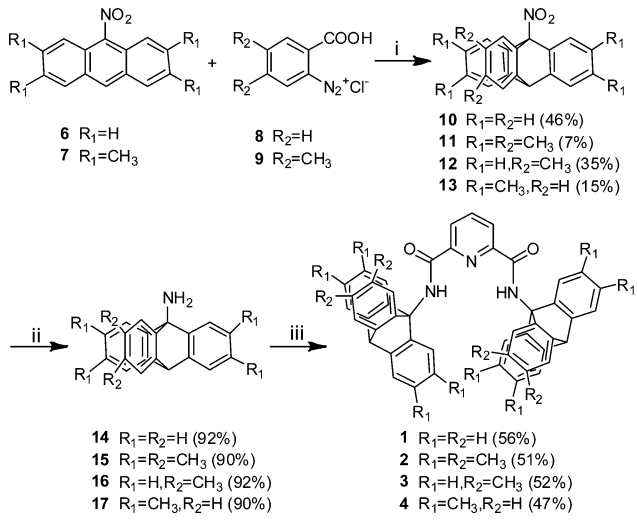

[a]Reagents and conditions: (i) 1,2-Epoxypropane, CH_2ClCH_2Cl, reflux; (ii) $SnCl_2$, HCl, CH_3COOH, reflux; (iii) 2,6-pyridinedicarboxylic dichloride, DIEA, CH_2Cl_2, rt (for **1**, **3**, and **4**); or 2,6-pyridinedicarboxylic acid, PyBOP, DMAP, DMF, reflux (for **2**).

benzenediazonium-2-carboxylate. For example, while 2,3,6,7,14,15-hexamethyl-9-nitrotriptycene (**11**) could be prepared from 2,3,6,7-tetramethyl-9-nitroanthracene (**7**) and 4,5-dimethylbenzenediazonium-2-carboxylate (**9**), reaction of **7** with 4,5-dimethylbenzenediazonium-2-carboxylate (**8**) gave 2,3,6,7-tetramethyl-9-nitrotriptycene (**13**). It was found that methyl substitution is detrimental to producing the desirable 9,10-adducts, probably because of the increased steric hindrance of the methyl group. Careful isolation of the adducts gave **11** in only 7% yield but a bit higher for **12** and **13**, 35% and 15%, respectively. Reduction[27] of **10**–**13** with $SnCl_2$ under acidic conditions provided the corresponding aminotriptycenes **14**–**17**. Amidation of **14** with 2,6-pyridinedicarboxylic acid chloride, using *N*,*N*-diisopropylethylamine (DIEA) as the base, gave the target compound **1** in a yield of 56%. However, the analogous convergent method to compound **2** was not successful, in which the reaction hardly proceeded even under reflux in toluene. Fortunately, **2** can be obtained in acceptable yield by the coupling of **15** and 2,6-pyridinedicarboxylic acid with the help of peptide coupling reagent benzotriazol-1-yloxytripyrrolidinophosphonium hexafluorophosphate (PyBOP). The final two target compounds **3** and **4** were prepared according to the method described for **1**. Structures of **1**–**4** are confirmed by NMR and high resolution mass spectra. The assignments of their experimental ^1H and ^{13}C NMR spectra were performed based on the corresponding ^1H–^{13}C HSQC, ^1H–^{13}C HMBC, ^1H–^1H NOESY, and ^1H–^1H COSY experiments (see Figures S2–S11 in SI).

X-ray Structures of 1 and 2. Crystal structure of **1** was obtained by slowly evaporating a solvent mixture of dichloromethane (DCM) and methanol at ambient temperature (Figure 2a). The crystal is an orthorhombic, solvent-contained system, with space group *P*2(1)2(1)2(1). Each unit cell contains four molecules of **1** and four of DCM, packed with high disorder. As expected, in the structure, the central bridge 2,6-pyridinedicarboxamido group adopted a preferred *cis* conformation ascribed to the hydrogen bonding between pyridine-N and amido-NH (the N–H···N(pyridine) distance of

DOI: 10.1021/acs.joc.5b01778
J. Org. Chem. 2015, 80, 11302–11312

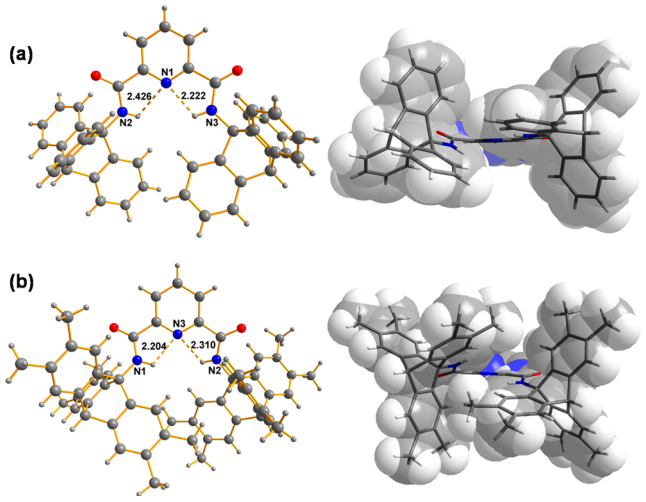

Figure 2. Ball and stick diagrams (left, top view) as well as the stick diagrams overlaid by Diamond 3.0-generated space-filling representation (right, side view) for molecular structures (a) **1** and (b) **2**, which crystallized from a mixture of dichloromethane and methanol. The dichloromethane molecules contained in the cell unit of **1** were omitted for clarity.

2.43 and 2.22 Å), holding the two Tp groups together to assemble a molecular bevel gear-like structure in C_2 conformation. The structure is not entirely symmetrical. While one amido group maintains a planar geometry with the core pyridyl group, the other is slightly twisted (with dihedral angles of 6°) to accommodate the sterics. Meanwhile, despite one blade (one phenyl ring) being directed *endo* in both rotators, the inward-facing ring in one rotator is more planar to the plane of pyridine (intersecting at an angle of 16°), but the counter one on the other Tp group is significantly more torsional (dihedral angles of 59°). The distances between the (9−9′) and (10−10′) bridgehead atoms of the Tp groups are 6.64 and 10.16 Å, respectively, providing a distance between the two centers of the Tp axles of about 8.4 Å, which is larger than the minimum axle−axle distances (7.0 Å) calculated by Siegel for a Tp-based molecular spur gear in C_2 conformation.[20] Notably, although by wireframe representation the two rotators seem separated, a space-filling mode (Figure 2a, right) reveals that they in fact partially stack upon each other, suggesting that they are able to achieve correlated motion, at least when **1** adopts ground-state conformation.

A single crystal of **2** can also be obtained from the solution in a mixture of dichloromethane and methanol (Figure 2b). The crystal is monoclinic, with a space group of $P2(1)/n$. Each unit cell contains only four molecules of **2**. Similar to that of **1**, the intramolecular hydrogen bonding constrains the methyl-subsitituted Tp groups, providing a gear-like structure in C_2 conformation, wherein the two amides are twisted and tilted up and down along the plane of pyridyl group with dihedral angles of 17° and 19°. The diminished planarity, compared to that of **1**, is ascribed to the bigger steric exclusion from the two methyl-subsitituted Tp groups when compared to that of unsubsitituted ones. The distances between the (9−9′) and (10−10′) bridgehead atoms of the Tp groups are 6.40 and 9.72 Å, which are a bit smaller than those in structure **1**. This is probably because of stronger π stacking and orbital interactions between the two Tp groups of **2**, as suggested by the fact that the distance between the planes of the two proximal benzene rings on one Tp group and the closest methyl protons on the counter Tp one is just about 3.05 Å. A space-filling mode (Figure 2b, right) clearly shows that the two Tp groups intermesh more tightly in comparison with that of **1**, providing the hope of possessing a higher efficiency of motion transmission.

Calculations. While some previous computational studies on molecular bear or spur gears directly focus on the molecular geometries and the relative energies of C_2, C_s, and C_{2v} conformations,[11−14,20] identification of the motion profile as well as the ground and the transition states within it for the studied system needs to include the most energetically favorable conformational transformation pathway, i.e., MEP, considering that the motions in the studied systems might be considerably different from those of the molecular gears. Therefore, starting from the X-ray structures, the unconstrained geometries of **1** and **2** were first optimized and confirmed to the global minima at DFT level of theory with the B3LYP hybrid functional and the 6-31G* basis set. Then, from this point, the MEPs were obtained by relaxed potential energy surface scan procedures[28,29] implemented in the GAUSSIAN 03 program package[30] as a function of the dihedral angle (denotes ϕ) of C_{17}(carbonyl)−N_{14}(amide)−C_{51}(bridgehead)−C_{70}(ring α) for **1** and C_{17}(carbonyl)−N_{14}(amide)−C_{47}(bridgehead)−C_{71}(ring α) for **2** (could be approximately regarded as the dihedral angle between the planes of benzene ring α and the adjacent carbonyl group) (Figure S17, Supporting Information). At each point on the MEPs, all the degrees of freedom other than the fixed dihedral angle were allowed to be fully optimized. Given the three-fold symmetry of the Tp group, the dihedral angle was scanned over 120° with a step size of 1°. To verify the transition states obtained by this scan strategy (scanned TSs), we reoptimized two transition states by using the conventional TS optimization method (to give optimized TSs) along the reaction pathways of the rotational isomerization of **1** and **2**. In this case, all the degrees of freedom are completely relaxed without any predefined reaction coordinates. All computational results are summarized in Figure 3 and Figure 4.

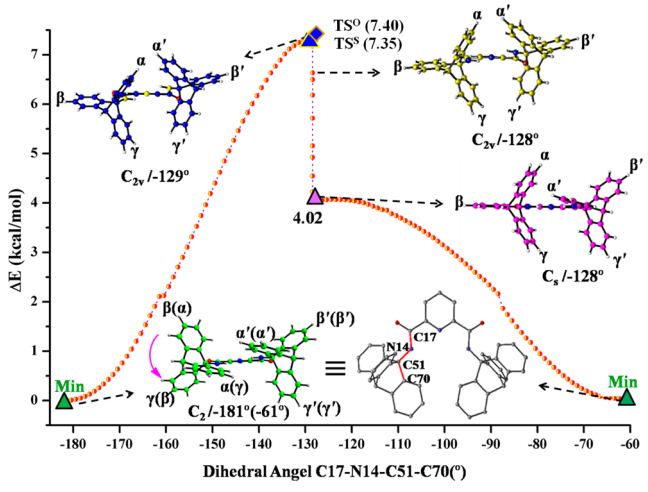

Figure 3. Minimum energy profile of rotational isomerization of **1** along C17−N14−C51−C70 (ϕ) dihedral angle calculated by a relaxed potential energy surface scan at the B3LYP/6-31G(d) level of theory. The transition states were calculated by scan strategy (TS^s) and the direction method of conventional TS optimization (TS°), respectively.

DOI: 10.1021/acs.joc.5b01778
J. Org. Chem. 2015, 80, 11302−11312

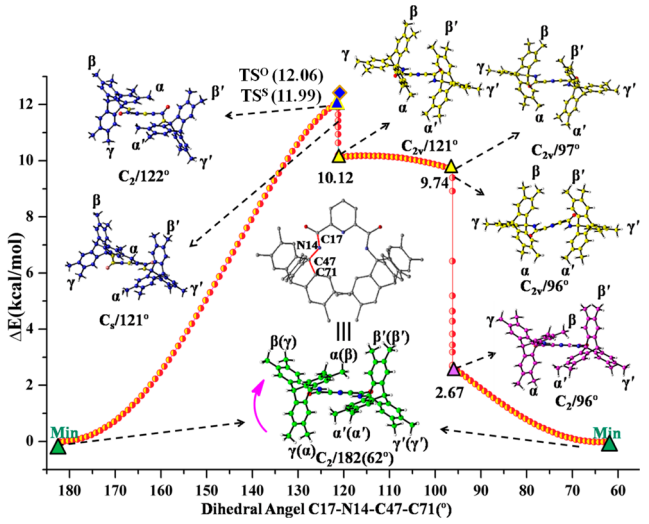

Figure 4. Minimum energy profile of rotational isomerization of **2** along C17−N14−C47−C71(ϕ) dihedral angle calculated by a relaxed potential energy surface scan at the B3LYP/6-31G(d) level of theory. The transition states were calculated by scan strategy (TS^{s}) and direction method of conventional TS optimization (TS^{o}), respectively.

The motion of **1** is predicted to start with gearing. DFT calculation confirms the C_2 conformation as the global minimum for **1** by vibrational analysis (Figure 3). The optimized geometry bears a close resemblance to the X-ray structure (Figure 2a). For example, the distances between the (9−9′) and (10−10′) bridgehead atoms of the Tp groups are predicted to be 6.88 and 10.62 Å, and the central bridged moiety 2,6-pyridinedicarboxamide is also almost planar. The dihedral angles between the planes of the two benzene rings directed *endo* (α and α', Figure 3) and the plane of the pyridyl group are measured to be 17.7° and 17.6°, indicative of a slightly more symmetrical structure when compared to that in the crystal.

Rotating the Tp moiety where benzene ring α located anticlockwise from ϕ dihedral angle of −181° gives rise to a slight distortion of the pyridylamides (Table S2, SI) and, more importantly, a disrotation of the counter Tp group, accompanied by a considerable increase in energy ascribed to the steric hindrance of carbonyl oxygen. The highest energy conformer of the energy curve, which shows up at the point where ϕ dihedral angle is −129° and is ca. 7.4 kcal mol^{-1} higher in energy than that in the minimum conformation, adopts an approximately gear-clashed C_{2v} orientation, suggesting that the gearing will lose fidelity soon. Notably, a temporary C═O···H−C hydrogen bond between the carbonyl oxygen and proton H_{38} on benzene ring β is predicted to be present in the process where ring β passes over the carboxyl group, and the strongest bonding (with H···O distance of 1.98 Å and H−C···O bond angle of 114.5°) occurs when these two groups are nearly coplanar, wherein ϕ = −129°. This hydrogen-bonding might be able to stabilize the C_{2v} transition state, thus, to some extent, lowering the rotational barrier of the Tp group.[31] Besides, the scanned TS shows negligible differences in geometric structure (deviation: 0.02−1.26°/dihedral angles; 0.0−0.002 Å/bond lengths) and relative energy (deviation: 0.05 kcal mol^{-1}) compared with the one obtained by the direct method of conventional TS optimizations (see Figure 3 and Table S4 in SI). Frequency calculation on this scanned TS yields one and only one imaginary frequency (41.67i cm^{-1}) corresponding to the rotational motion of triptycene along the axle of the C(triptycene)−N(amide) bond, which is very close to the optimized TS (41.75i cm^{-1}) with the same vibration mode. Intrinsic reaction coordinate (IRC) calculations starting from optimized or scanned TSs confirm that these energy maxima unambiguously connect with the corresponding reactant of ground-state minima along the reaction paths of triptycene rotation along the axles of the C−N bond. These suggest that there are no principal differences in describing the rotational isomerization of triptycene by using the scan strategy and the direct method of transition state optimization and also indicate that it is reasonable to choose C17−N14−C51−C70 dihedral angle as the reaction coordinate in the MEP calculations of this rotational isomerization. As expected, with just a slightly continuous rotation of the driving Tp group from −129° to −128°, the gear slips and the counter Tp group rotates back (anticlockwise), accompanied by a drastic reduction (3.3 kcal mol^{-1}) in energy. The reverse rotation is ascribed to the relatively too large interaxle distance as well as to the rotation barrier for the counter Tp rotator. Another important transition geometry, which adopts an approximate C_s conformation, is observed at ϕ = −128°, in which the dihedral angle between the planes of ring α' and the pyridyl group is 13°, pretty close to that in the minimum conformation. With further rotation of the driving Tp rotator to the final where ϕ = −61°, the counter Tp moiety keeps almost stable, while the energy moderately decreases. These computational results clearly show that rotation of one Tp rotator on **1** would give rise to a vibration of the counter one, indicating that rotation-derived vibration is the main mode of the intramolecular motion of **1** as we designed.

In contrast to **1**, the DFT calculation on molecule **2** predicts a slightly more complicated intramolecular movement profile (Figure 4). The global minimum of **2** possesses a C_2 conformation and closely resembles its single crystal geometry (Figure 2b), wherein the central 2,6-pyridine dicarboxamide moiety is planar and the dihedral angles between this moiety and both the plane of benzene ring α and α' are 23°. At this state, the ϕ dihedral angle was measured to be 182°. Different from that of **1**, clockwise rotation of the Tp group where benzene ring α is located initially gives a distortion of the adjacent amide and a gradual increase in energy but does not induce perceptible anticlockwise rotation of the counter Tp group. This is probably ascribed to the big methyl-substituted Tp rotators, which are larger in radius than the minimum axle−axle distance required for the C_s orientation so that the pyridylamide connected to the driving rotator should at first deform to accommodate the crescent sterics. The highest energy comformer, which lies ca. 12.0 kcal mol^{-1} higher in energy level than that of the global minium, shows up at ϕ = 122°, where the pyridylamide connected with the driving rotator is seriously distorted while the counter Tp-amide is almost still under the equilibrium position. Similar to the case of **1**, the highest energy conformer obtained by scan strategy (i.e., TSs) is very close to the one computed by conventional TS optimizations along the unbiased reaction coordination of **2** (Table S5). This reveals that the rotational isomerization that proceeds along the axle of the C(triptycene)−N(amide) bond is the predefined reaction coordinate in our scan strategy. Continuous rotation of the driving rotator leads to an apparent disrotatory motion of the counter Tp group, through anticlockwise rotation of the counter Tp group around C_{23}(Tp)−N(amide) bonds as well as the deformation of the

DOI: 10.1021/acs.joc.5b01778
J. Org. Chem. 2015, 80, 11302−11312

connected pyridylamide (Table S3, SI). The strain in the whole molecule thus gets released, giving a sharp decrease in the energy. Surprisingly, in the range of ϕ = 121−97°, rotation of the driving rotator once again produces only the deformation of the connected amide, which gives rise to a transient increase in the interaxle distance and a slight decrease in energy. Subsequently, through a gear-clashing transition (C_{2v}/96°, Figure 4), the position of benzene ring α and α' reverses, providing a new transition structure in which the counter Tp almost returns back to its equilibrium position. This is distinctly different from what we hypothesized, as we expected that the methyl substituents would increase the size of rotator's blade, thus benefiting gearing. Obviously, the rotation barrier of the Tp group was underestimated in our design. In fact, this barrier is so high that the molecule prefers to weaken the N−H···N (pyridine) hydrogen-bonding and distort the amide group to create slippage rather than overcome an additional rotation barrier from the counter rotator. Further rotation of the driving Tp group from ϕ = 96° releases the strain arising from the torsion of pyridylamides, providing a moderate decrease in energy until finally a global minimum geometry is reobtained. All these predict that the methyl substituents will not change the basic mode of motion of **1** but will increase the energy barrier of slippage, thus raising the free energy of activation for the overall motion transmission.

VT-NMR Experiments of 1 and 2. Experimental studies on the motions of **1** and **2** in solution were carried out with NMR spectroscopy rather than other methods, such as time-resolved emission spectroscopy[32] (internal rotation in the studied molecules would be too slow on the time scale of fluorescence emission, giving fluorescence lifetimes that are generally on the order of 1−10 ns). At ambient temperature, the Tp groups rotate fast around C_9 (Tp)−N(amide) bonds on the NMR time scale, giving the six benzyl rings on Tp moieties that are magnetically equivalent. Consequently, the ^{1}H NMR spectrum of **1** in CD_2Cl_2 at 298 K shows only one set of sharp signals for the benzyl rings (i.e., two doublets at 7.48 and 7.54 ppm are assigned to protons H_1 and H_4 as well as two triplets at 7.02 and 7.12 ppm for H_2 and H_3, respectively). In addition, the amide protons exhibit one single signal at 9.61 ppm as well. In the corresponding ^{1}H−^{1}H NOESY spectrum (Figure S2), the cross-peaks between amide protons and their neighboring pyridinyl protons are completely absent, demonstrating that the central bridge 2,6-pyridinedicarboxamide unit is mainly rotationally constrained in solution as that in the solid structure.

To explore more dynamic features of **1** in CD_2Cl_2, variable-temperature (VT) ^{1}H NMR investigations were then carried out (Figure 5a and Figure S18). While the pyridyl protons signals of **1** show no changes at all upon the decrease in temperature in the range examined (Figure S18), the Tp protons, especially the protons H_1 and H_2 close to the counter Tp rotator, undergo a slight upfield and downfield shift, respectively, at the beginning of this process. The changes in the chemical shift are ascribed to the increase in the fraction of **1** in the ground-state conformation. Decreasing the temperature further provides considerable broadening of H_1 and H_2, clearly indicating that the Tp−N rotations slow upon lowering the temperature. A decoalescence of H_1 and H_2 was observed at 203 K. This comparatively high coalescence temperature in comparison with all those tightly meshed molecular gears[12a] is due to the steric hindrance of the carbonyl oxygen atom as well as the slippage process, arising from the energy barrier to Tp−N rotations. With an even further decrease in the temperature,

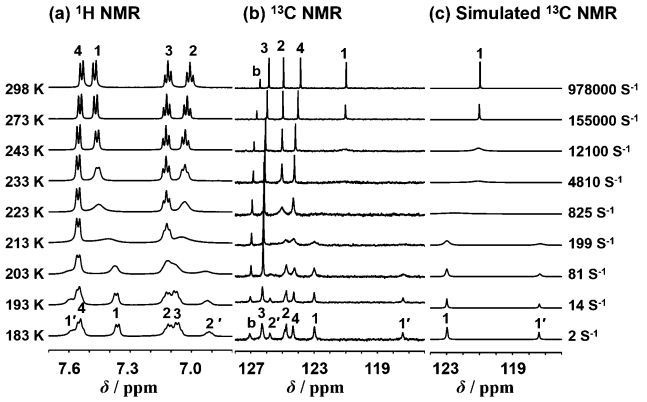

Figure 5. (a) Partial VT ^{1}H NMR spectra (500 MHz) of **1** (2 mM) in CD_2Cl_2. (b) Partial VT ^{13}C NMR spectra (125 MHz) of **1** (40 mM) in CD_2Cl_2. (c) Simulated VT ^{13}C NMR spectra at the region of carbon C_1, which were obtained with DNMR Line Shape Analysis procedure implemented in the Topspin 2.1 program.[33] The temperature (K) and calculated interconversion rate constants (k_r, s^{-1}) are given for each trace.

the rotation of the Tp groups becomes frozen and thus either of the H_1 and H_2 signals splits into two peaks, with an intensity ratio of 2:1. The ^{1}H NMR spectra in this case mainly correspond to **1** in ground-state conformation, where the protons H_1 and H_2 show small peaks at 7.58 and 6.91 ppm, respectively, which can be assigned to the relevant protons on the inward-facing benzene rings (labeled as α and α' in Figure 3), and larger peaks at 7.36 and 7.11 ppm, respectively, to the corresponding protons on the other four rings. The smaller peak of the H_2 signal is upfield from the bigger one, which is ascribed to ring-current effects arising from π-stacking interaction between rings α and α'. In contrast, the signals of H_1 on rings α and α' locate downfield, which is probably ascribed to the deshielding of pyridine-N (3.57 Å for the distance of C_1−N(pyridyl) in the crystal structure). Expectedly, the benzene rings β and γ are not chemically equivalent in the case of **1** in the ground state as predicted by DFT calculation (Figure 3), as evidenced by the signals of H_1 at 7.36 ppm and H_2 at 7.11 ppm that split further when the temperature is as low as 183 K. It is noteworthy that, in the whole process, the chemical shift of the amide proton remains almost unchanged ($\Delta\delta$ = 0.07 ppm) (Figure S18), which indicates that, throughout the entire range of temperature examined, the intramolecular H-bonding between the pyridine-N and the amide is always present and that the N−H···N (pyridine) bonding pattern (including the bond angle and bond distance) does not change much upon the change of temperature. This is important because it once again experimentally demonstrates that the molecule keeps adopting a gear-like conformation in the motion, as previously indicated by the ^{1}H−^{1}H NOESY spectrum.

The mulitiplicity and overlap of some important proton signals of **1** prevent a direct line-shape analysis of the ^{1}H NMR spectra for elucidating the kinetic parameters for the motions of **1**. To circumvent this problem, a VT ^{13}C NMR experiment was carried out (Figure 5b and Figure S19).[34] Similar to that of the VT ^{1}H NMR experiment, upon lowering the temperature, the signals of C_1 and C_2 gradually broaden and decoalesce at about 213 K. At 183 K, two pair of sharp peaks with a 2:1 ratio in intensity for C_1 and C_2 were observed. The rate constant corresponding to the process where any one of the benzene

DOI: 10.1021/acs.joc.5b01778
J. Org. Chem. 2015, 80, 11302−11312

rings passes over the carbonyl group were derived from the line-shape analyses of the C_1 resonances (Figure 5c). From these constants, the free energy of activation ($\Delta G^{\ddagger}$) as well as the enthalpy ($\Delta H^{\ddagger}$) and entropy ($\Delta S^{\ddagger}$) were derived from the Eyring plots[35] (Table 1, Figure S20), in which $\Delta G^{\ddagger}$ is

Table 1. Summary of the Thermodynamic Parameters for 1−4

compd	N_{methyl}[a]	$\Delta G^{\ddagger}_{298\ K}$ (kcal mol^{-1})	$\Delta H^{\ddagger}$ (kcal mol^{-1})	$\Delta S^{\ddagger}$ (cal mol^{-1} K^{-1})
1[b]	0	9.0 ± 1.0	12.3 ± 0.4	11.0 ± 2.0
2[c]	12	11.0 ± 0.2	9.2 ± 0.1	−5.9 ± 0.4
2[b]	12	11.0 ± 0.2	9.2 ± 0.1	−5.9 ± 0.3
3[b]	4	9.0 ± 0.7	12.3 ± 0.3	11.0 ± 1.2
4[c]	8	10.8 ± 0.4	8.9 ± 0.2	−6.3 ± 0.7

[a]Number of methyl substituents on the molecule. [b]These values were obtained from VT ^{13}C NMR experiments. [c]These values were obtained from VT ^{1}H NMR experiments.

calculated to be 9.0 kcal mol^{-1} that is pretty close to the DFT-calculated energy gap between the transition state (TS^s and TS^o) and the minimum conformers.

We next performed VT ^{1}H and ^{13}C NMR experiments on **2** in CD_2Cl_2 (Figure 6, Figures S21, S23, and S24). Similar to that

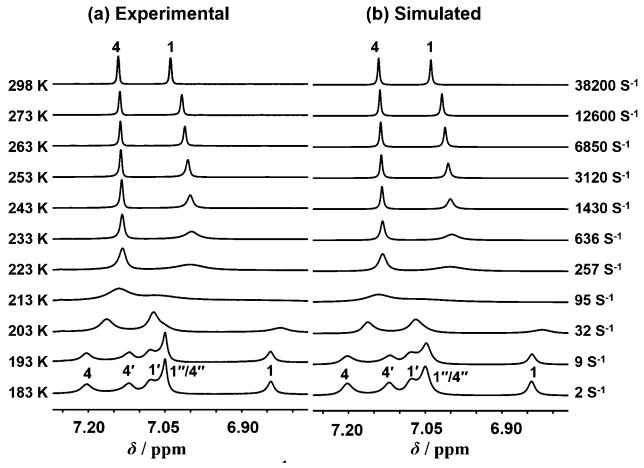

Figure 6. (a) Experimental and (b) simulated VT ^{1}H NMR spectra (500 MHz) of **2** (2 mM) at the region of H_1 and H_4 in CD_2Cl_2. The temperature (K) and calculated interconversion rate constants (k_r, s^{-1}) are given for each trace.

of **1**, decreasing the temperature slows and finally freezes the rotation of the methyl-substituted Tp groups, giving rise to broadening followed by splitting of the signals of the protons and carbons which are spatially close to the counter Tp group. In this process, the chemical shift of amido-NH just slightly downshifts ($\Delta\delta$ = 0.15 ppm) (Figure S21), which suggests that, similar to that of **1**, the amides are H-bonded with pyridine-N all the time but might be slightly more distorted at ambient temperature compared to that of **1** statistically. A decoalescence is observed at ca. 213 K for both proton H_1 and carbon C_1, wherein the signals split into two peaks with a 2:1 ratio in intensity. Another decoalescence is found to be around 193 and 183 K for H_1 and C_1, respectively, in which the resonances split further and exhibit three distinguishable peaks as expected. Line-shape analysis of the VT ^{1}H NMR spectra provides the rate constant of the rotation (Figure 6), which shows that, while the rotation of **2** is as frozen as that of **1** at 183 K, increasing the temperature gives rise to an increase (but less dramatic than that of **1**) in the rotational speed. All these observations indicate that the rotational barrier of the substituted-Tp groups in **2** is a bit higher than that of Tp groups in **1**. Two sets of corresponding thermodynamic parameters were thus derived independently from the VT ^{1}H and ^{13}C NMR spectra (Figures S22 and S26). Both approaches provide very consistent results of 11.0 kcal mol^{-1} (Table 1),[36] which is again consistent with that of the DFT-calculated results (TS^s and TS^o).

The fact that $\Delta G^{\ddagger}$ for the rotation in molecule **2** is just slightly larger than that in the case of **1** suggests that both molecules do not tend to gear but motion in a way as predicted by DFT calculation. This is because the methyl substituent would not affect the rotation of the whole Tp rotator around C_9(Tp)−N(amide) bonds but only the interaction between two Tp groups while motioning. Consequently, if both molecules keep gearing, their free energy of activation would be very close, given the gearing itself almost unhindered. Besides, it is not likely that **2** keeps gearing while **1** undergoes continuous slippage, since in such a case, molecule **2** needs to overcome the rotation barrier for one more Tp rotator, which would give rise to considerable increase in the free energy of activation when compared to that of **1**. In both cases, $\Delta H^{\ddagger}$ is predominant over $\Delta S^{\ddagger}$ in its contribution to $\Delta G^{\ddagger}$, indicating that the rotation is mainly enthalpically disfavorable. The negative value of $\Delta S^{\ddagger}$ in the case of **2** suggests that molecule **2** in the transition states has totally less degree of freedom when compared to that in the ground state; probably in such cases, the vibration of some subunits are partially restricted by the torsional strains.

X-ray Structures and Dynamic Behavior of 3 and 4. The crystal structure of **3** was obtained by slowly evaporating the acetonitrile solvent at ambient temperature (Figure S12a). The crystal is a monoclinic system, and there are four molecules of **3** and four of acetonitrile in each unit cell. The geometry is highly symmetrical, with two benzene rings having a methyl substituent located at the flank. The distances between the (9−9′) and (10−10′) bridgehead atoms of the Tp groups are 7.05 and 11.24 Å, respectively, indicating that the two Tp groups possess a larger axle−axle distance compared to that of **1** crystallized from the solution mixture of DCM and methanol. This larger axle−axle distance is probably induced by cocrystallized acetonitrile molecules in the crystal package, as we later found that the crystal structure of **1** cocrystallized with acetonitrile can also be successfully obtained from acetonitrile solution and the structure possesses an axle−axle distance larger than that of the one grown in a mixture of DCM and methanol (Figure S12c). The larger interaxle distance is favorable for releasing the steric repulsion between Tp groups, which leads to an approximate C_{2v} conformation in the geometry of **3** wherein the dihedral angles between the planes of two benzene rings directed *endo* and the plane of pyridyl group are as small as 2° and 7°, respectively.

Crystals of **4** grown in a mixture of DCM and methanol also show a symmetrical structure, in which the two benzene rings without methyl substituents directly flank unexpectedly (Figure S12b). There are two molecules of **4** and four of methanol in each unit cell. Nevertheless, the distances between the (9−9′) and (10−10′) bridgehead atoms of the Tp groups are as short as 6.25 and 9.46 Å, respectively, indicative of a compact

DOI: 10.1021/acs.joc.5b01778
J. Org. Chem. 2015, 80, 11302−11312

conformation slightly more than those in the other studied crystal structures.

Since the X-ray structures of **3** and **4** skeletally resemble closely those of **1** and **2** (Figures S13 and S14), we then carried out dynamic NMR studies for better understanding of the dynamic properties of this type of molecule. Due to the fast rotation of Tp groups at ambient temperature, the ^{1}H NMR spectrum of **3** in CD_2Cl_2 at 298 K shows only one set of sharp signals of the amides and the benzene rings without methyl substituents (Figure S27). Decreasing the temperature below 233 K gives rise to broadening of all Tp signals and splitting of the signals of unsubstituted benzene rings, wherein the decoalescences of H_1 and H_2 occur at ca. 203 K. Notably, in this process, decoalescences of amide-NH and pyridonyl protons were observed at 193 K, which are ascribed to the appearance of phase isomers (Figures S35 and S36). The splitting of Tp signals arising from the presence of phase isomers is difficult to distinguish due to the overlap of signals. Integration analysis shows that two phase isomers exist in ca. 2:1 ratio, consistent with the observation for most molecular gear systems.[11b,18] Similar phenomena could also be observed in the corresponding VT ^{13}C NMR spectra, wherein decoalescences of several Tp carbons such as C_1 and C_2 are observed at ca. 213 K and the phase isomers start to show up at ca. 203 K (Figures S28 and S29). Clearly, in both the VT ^{1}H and ^{13}C NMR experiments, the signals of Tp groups decoalesce at a bit higher temperature when compared to that of the appearance of the phase isomers. This is understandable. Given that the energy barrier for vibration is much lower than that for rotation, even under certain conditions where the rotation of Tp rotators is freezing, it is still possible for the vibration to take place, providing the possibility of slippage, thus inhibiting the appearance of phase isomers. Consequently, for the studied cases, decoalescence of Tp signals might not always synchronize with that of amides, especially for systems which possess rotators with short blades such as **3**. On the other hand, the fact that the phase isomers could not be observed above 203 K indicates that the two Tp rotators keep slipping in those cases, providing evidence that the rotation of the driving rotator gives a vibration of the counter one. Calculation of the thermodynamic parameters for Tp rotation was based on the changes in signal line shape of carbon C_{11} upon the decrease of temperature (Figures S30 and S31), in which the range of temperature was carefully chosen as 263−193 K to avoid the effect of the presence of phase isomers. The resultant data are listed in Table 1.

For molecule **4** possessing more methyl substituents, the decoalescences of amide-NH and pyridonyl protons show up at temperatures as high as ca. 213 K (Figure 7). The signal of methyl protons H_{m2} decoalesces at ca. 223 K, indicative of the presence of slipping caused by the vibration of Tp groups as expected. The decoalescence of Tp signals is difficult to identify at 213 K due to the serious broadening but can be clearly observed at 203 K, although those signals could not be precisely assigned in such cases. The nonequivalence of two benzene rings with methyl substituents as well as the appearance of phase isomers gives rise to a very complicated ^{1}H NMR spectrum of **4** at low temperature such as 193 and 183 K. Nevertheless, the ratio of two phase isomers could still be obtained by integration of split amide-NH signals, which gives a ratio of ca. 1.2:1 rather than 2:1, probably because the *meso* isomers have lower potential energy in the ground state when compared to the *dl* ones (Figures S37 and S38). The changes in

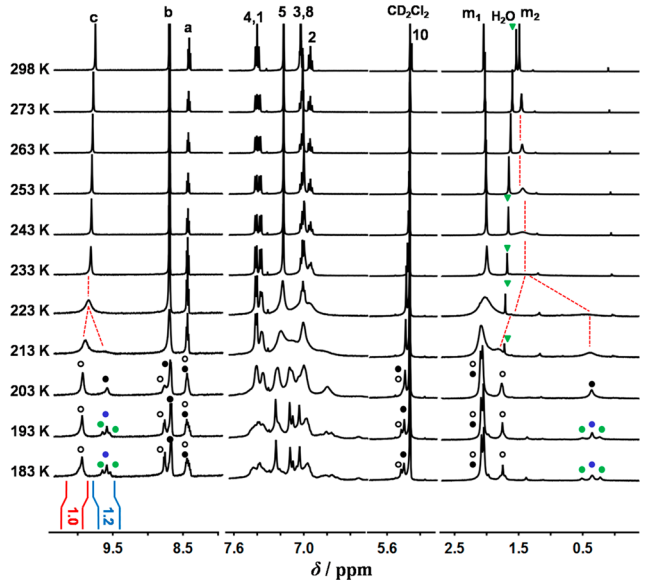

Figure 7. Partial VT ^{1}H NMR spectra (500 MHz) of **4** (2 mM) in CD_2Cl_2. The circles in different colors indicate signals of a different set of isomers. The splitting of Tp signals arising from the appearance of phase isomers is difficult to distinguish due to the overlap of signals.

signal of methyl protons H_{m1} and H_{m2} upon the decrease of temperature from 263 to 203 K were used to calculate the thermodynamic parameters for the Tp rotation (Figures S33 and S34). As shown in Table 1, the values of kinetic parameters in the case of **4** approximate those of **2**, while the values of **3** are close to those of **1**. This suggests that, in terms of the motion transformation between the two Tp components in the studied systems, combination of the unsubstituted Tp group and the one with six methyl substituents might provide dynamic properties similar to that of **2**.

Notably, despite both the DFT calculation and VT-NMR experiments indicating a rotation-driven vibration as the most energy-economical way for the motion of **1**, for real molecules in solution, the driving rotator would not be preselected and fixed, and a geared rotation might still be possible (especially at high temperature) if the molecule possesses high enough energy for both Tp groups to overcome their respective rotation barriers. Besides, the thermally stimulated motions should occur without direction bias, giving the three-fold symmetry of Tp groups and the absence of any processes of chiral discrimination.[8b]

■ CONCLUSIONS

In summary, we have designed and synthesized a series of N^2,N^6-bis(triptycene-9-yl)pyridine-2,6-dicarboxamides **1**−**4**, which are derived from conventional molecular gears. DFT and dynamic NMR experiments have indicated that this kind of molecule possesses dynamic properties different from those of the molecular gears, wherein one triptycene rotator rotates around the C(Tp)−N(amide) bond while the other one maintains an associated rocking vibration through an intermediate slippage process. Enlarging the blades of rotators with methyl substituents increases the free energy of activation but would not change the mode of the motion. Our studies thus provide a conceptual approach to design molecular transmission devices that are capable of transforming the mode of motion from rotation to rocking vibration.

DOI: 10.1021/acs.joc.5b01778
J. Org. Chem. 2015, 80, 11302−11312

EXPERIMENTAL SECTION

All starting chemicals were obtained from commercial sources and used without further purification. Anhydrous dichloromethane (DCM) was distilled over calcium hydride (CaH_2) under inert atmosphere. NMR spectra were obtained with a 400, 500, or 600 MHz spectrometer using chloroform-*d* ($CDCl_3$), dichloromethane-d_2 (CD_2Cl_2), methanol-d_4 (CD_3OD), and acetone-d_6 as the solvents. The chemical shift references were as follows: (^{1}H) chloroform-*d*, 7.26 ppm; (^{13}C) chloroform-*d*, 77.16 ppm (chloroform-*d*); (^{1}H) dichloromethane-d_2, 5.32 ppm; dichloromethane-d_2, 53.52 ppm; (^{1}H) methanol-d_4, 3.31 ppm, (^{1}H) acetone-d_5, 2.05 ppm. High resolution mass spectra (EI and ESI) were acquired on a GCT, FT-ICR spectrometer. IR spectra were recorded on an FT-IR spectrometer with a thin KBr disk.

9-Nitro-2,3,6,7-tetramethylanthracene (7). To a solution of 2,3,6,7-tetramethylanthracene[37] (190 mg, 0.8 mmol) in CH_2Cl_2 (19 mL) was added an aqueous HNO_3 solution (20%, 19 mL). The mixture was refluxed for 4 h. The reaction mixture was diluted with water (10 mL) and extracted with CH_2Cl_2 (3 × 10 mL). The combined organic extracts were dried over Na_2SO_4 and then concentrated under reduced pressure. Compound **7** (212 mg, 95%) was obtained as a yellow solid. R_f = 0.6 (petroleum ether (PE)/CH_2Cl_2 = 2/1). Mp = 190−192 °C. IR (KBr): 2918, 2850, 1643, 1531, 1460, 1444, 1384, 1327, 1116, 898 cm^{-1}. ^{1}H NMR (400 MHz, $CDCl_3$), δ = 8.32 (s, 2H), 7.74 (s, 2H), 7.65 (s, 2H), 2.47 (s, 6H), 2.46 (s, 6H); ^{13}C NMR (100 MHz, $CDCl_3$), δ = 139.4, 136.2, 130.1, 127.8, 127.2, 121.8, 120.2, 21.0, 20.3. HRMS (EI-TOF) *m*/*z*: [M]$^+$ calcd for 279.1259 (100%, $C_{18}H_{17}NO_2$), found 279.1263 (100%, 1.3 ppm).

4,5-Dimethylbenzenediazonium-2-carboxylate (9). To a mechanically stirred suspension of 4,5-dimethylanthranilic acid (825 mg, 5 mmol) in ethanol (50 mL) in an ice−water bath was added dropwise concentrated hydrochloric acid (0.63 mL), followed by the addition of isopentyl nitrite (1.35 mL). After the mixture was stirred for 15 min, diethyl ether (150 mL) was added. Then the reaction mixture was stirred for another 30 min. The product was filtered and washed with diethyl ether to give the product, 975 mg (92%), which was used without further purification.

General Methodology for the Synthesis of Compounds 10−13. The procedure for the synthesis of triptycene or derivatives was followed as previously reported:[38] Benzyne (**8**[39] or **9**) (7−10 mmol) was added in portions to a mixture of 9-nitroanthracene or its derivative **7** (1 mmol) and 1,2-epoxypropane (2 mL) in dichloroethane (30 mL) and refluxed 24 h. The reaction mixture was concentrated under reduced pressure. Then the resultant solid was washed with methanol. The residue was purified by silica gel column chromatography.

9-Nitrotriptycene (10). Purification by silica gel column chromatography (PE/CH_2Cl_2 = 3/1) to give compound **10** (137 mg, 46%) as a white solid. R_f = 0.5 (PE/CH_2Cl_2 = 3/1). Mp = 246−248 °C. IR (KBr): 3072, 3038, 2968, 1543, 1459, 1446, 1365, 1295, 1156, 872, 803, 752, 620 cm^{-1}. ^{1}H NMR (400 MHz, $CDCl_3$), δ = 7.67−7.71 (m, 3H), 7.42−7.46 (m, 3H), 7.09−7.14 (m, 6H), 5.42 (s, 1H); ^{13}C NMR (100 MHz, $CDCl_3$), δ = 143.8, 140.4, 126.9, 125.8, 123.7, 122.1, 96.9, 54.0. HRMS (EI-TOF) (*m*/*z*) [M]$^+$ calcd for 299.0946 (100%, $C_{20}H_{13}NO_2$), found 299.0950 (100%, 1.2 ppm). Lit.[26a] Yield: 33%; ^{1}H NMR ($CDCl_3$), δ = 7.68 (m, 3H), 7.44 (m, 3H), 7.07−7.15 (m, 6H), 5.41 (s, 1H).

2,3,6,7,14,15-Hexamethyl-9-nitrotriptycene (11). Purification by silica gel column chromatography (PE/CH_2Cl_2 = 3/1) to give compound **11** (27 mg, 7%) as a white solid. R_f= 0.5 (PE/CH_2Cl_2 = 3/1). Mp = 258−260 °C. IR (KBr): 3010, 2958, 2920, 2853, 1548, 1465, 1384, 1362, 1271, 866, 809, 604 cm^{-1}. ^{1}H NMR (400 MHz, $CDCl_3$), δ = 7.41 (s, 3H), 7.16 (s, 3H), 5.17 (s, 1H), 2.17 (s, 9H), 2.16 (s, 9H); ^{13}C NMR (100 MHz, $CDCl_3$), δ = 141.9, 138.6, 137.1, 135.5, 134.7, 133.4, 124.7, 123.0, 122.8, 96.7, 52.7, 19.8, 19.5. HRMS (EI-TOF) (*m*/*z*) [M]$^+$ calcd for 383.1885 (100%, $C_{26}H_{25}NO_2$), found 383.1884 (100%, −0.3 ppm).

2,3-Dimethyl-9-nitrotriptycene (12). Purification by silica gel column chromatography (PE/CH_2Cl_2 = 3/1) to give compound **12** (115 mg, 35%) as a white solid. R_f = 0.5 (PE/CH_2Cl_2 = 3/1). Mp = 235−238 °C. IR (KBr): 3067, 2963, 2921, 1545, 1460, 1383, 1364, 1292, 868, 805, 760, 745, 662 cm^{-1}. ^{1}H NMR (400 MHz, $CDCl_3$): δ = 7.65−7.67 (m, 2H), 7.45 (s, 1H), 7.40−7.42 (m, 2H), 7.23 (s, 1H), 7.08−7.10 (m, 4H), 5.33 (s, 1H), 2.19 (s, 3H), 2.18 (s, 3H); ^{13}C NMR (100 MHz, $CDCl_3$), δ = 144.1, 140.7, 138.0, 135.1, 141.3, 133.8, 126.8, 125.6, 125.0, 123.5, 123.3, 121.9, 96.9, 53.6, 19.9, 19.5. HRMS (EI-TOF) (*m*/*z*) [M]$^+$ calcd for 327.1259 (100%, $C_{22}H_{17}NO_2$), found 327.1256 (100%, −1.0 ppm).

2,3,6,7-Tetramethyl-9-nitrotriptycene (13). Purification by silica gel column chromatography (PE/CH_2Cl_2 = 3/1) to give compound **13** (53 mg, 15%) as a white solid. R_f = 0.5 (PE/CH_2Cl_2 = 3/1). Mp = 232−235 °C. IR (KBr): 3065, 3038, 2918, 1634, 1548, 1463, 1383, 1361, 1272, 756, 613 cm^{-1}. ^{1}H NMR (400 MHz, $CDCl_3$), δ = 7.64 (t, 1H, *J* = 4.2 Hz), 7.44 (s, 2H), 7.38 (t, 1H, *J* = 4.2 Hz), 7.20 (s, 2H), 7.06−7.08 (m, 2H), 5.26 (s, 1H), 2.18 (s, 6H), 2.17 (s, 6H); ^{13}C NMR (100 MHz, $CDCl_3$), δ = 144.4, 141.7, 141.0, 138.3, 134.9, 133.7, 126.7, 125.6, 124.9, 123.3, 123.2, 121.8, 96.8, 53.2, 19.9, 19.5. HRMS (EI-TOF) (*m*/*z*) [M]$^+$ calcd for 355.1572 (100%, $C_{24}H_{21}NO_2$), found 355.1570 (100%, −0.6 ppm).

General Methodology for the Synthesis of Compounds 14−17. Reduction of compounds **10**−**13** with $SnCl_2$/HCl according to the procedure reported in the literature[27] afforded compounds **14**−**17** with good yields.

9-Triptycylamine (14). Compound **14** was obtained as a white solid in 92% yield. R_f = 0.3 (PE/ethyl acetate = 2/1). Mp = 212−214 °C. IR (KBr): 3442, 3385, 3067, 2951, 1617, 1455, 1296, 1130, 749, 633 cm^{-1}. ^{1}H NMR (400 MHz, $CDCl_3$), δ = 7.49 (d, 3H, *J* = 7.3 Hz), 7.40 (d, 3H, *J* = 6.9 Hz), 7.01−7.09 (m, 6H), 5.43 (s, 1H), 2.61 (br, 2H); ^{13}C NMR (100 MHz, $CDCl_3$), δ = 146.8, 145.1, 125.4, 125.2, 123.4, 119.5, 64.3, 53.4. HRMS (ESI-FT-ICR) [M + H]$^+$ calcd for 270.127726 (100%, $C_{20}H_{16}N$), found 270.127790 (100%, −0.2 ppm). Lit.[26a] Yield: 91%; ^{1}H NMR ($CDCl_3$), δ = 7.48 (m, 3H), 7.38 (m, 3H), 7.06 (m, 3H), 7.01 (m, 3H), 5.409 (s, 1H), 2.607 (br, 2H).

2,3,6,7,14,15-Hexamethyl-9-triptycylamine (15). Compound **15** was obtained as a white solid in 90% yield. R_f = 0.3 (PE/ethyl acetate = 2/1). Mp = 290−292 °C. IR (KBr): 3439, 3373, 3004, 2957, 2917, 2854, 1626, 1465, 1383, 1284, 996, 865, 622 cm^{-1}. ^{1}H NMR (400 MHz, $CDCl_3$), δ = 7.21 (s, 3H), 7.13 (s, 3H), 5.19 (s, 1H), 2.56 (br, 2H), 2.16 (s, 9H), 2.14 (s, 9H); ^{13}C NMR (100 MHz, $CDCl_3$), δ = 144.8, 143.2, 132.9, 132.6, 124.7, 120.8, 63.4, 52.0, 19.7, 19.5. HRMS (ESI-FT-ICR) (*m*/*z*) [M + H]$^+$ calcd for 354.221626 (100%, $C_{26}H_{28}N$), found 354.221764 (100%, −0.4 ppm).

2,3-Dimethyl-9-triptycylamine (16). Compound **16** was obtained as a white solid in 92% yield. R_f = 0.3 (PE/ethyl acetate = 2/1). Mp = 216−218 °C. IR (KBr): 3375, 3319, 3000, 2957, 2915, 1629, 1456, 1383, 1269, 1025, 913, 884, 806, 759, 739, 621 cm^{-1}. ^{1}H NMR (400 MHz, CD_3OD), δ = 7.48 (d, 2H, *J* = 6.8 Hz), 7.34 (d, 2H, *J* = 6.8 Hz), 7.27 (s, 1H), 7.15 (s, 1H), 6.96−7.04 (m, 4H), 5.35 (s, 1H), 2.20 (s, 3H), 2.17 (s, 3H); ^{13}C NMR (100 MHz, $CDCl_3$), δ = 147.2, 145.4, 144.3, 142.8, 133.2, 132.9, 125.3, 125.1, 123.3, 121.1, 119.4, 119.3, 64.1, 52.9, 19.8, 19.6. HRMS (ESI-FT-ICR) (*m*/*z*) [M + H]$^+$ calcd for 298.159026 (100%, $C_{22}H_{20}N$), found 298.159170 (100%, −0.5 ppm).

2,3,6,7-Tetramethyl-9-triptycylamine (17). Compound **17** was obtained as a white solid in 90% yield. R_f = 0.3 (PE/ethyl acetate = 2/1). Mp = 212−214 °C. IR (KBr): 3444, 3374, 3007, 2921, 2852, 1627, 1454, 1383, 1261, 1021, 803, 621 cm^{-1}. ^{1}H NMR (400 MHz, $CDCl_3$), δ = 7.43 (d, 2H, *J* = 7.2 Hz), 7.33 (d, 2H, *J* = 7.2 Hz), 7.24 (s, 1H), 7.16 (s, 1H), 6.96−7.05 (m, 2H), 5.27 (s, 1H), 2.56 (br, 2H), 2.18 (s, 3H), 2.16 (s, 3H); ^{13}C NMR (100 MHz, $CDCl_3$), δ = 147.4, 145.7, 144.6, 143.0, 133.0, 132.8, 125.3, 125.0, 124.9, 123.1, 120.9, 119.1, 63.8, 52.5, 19.8, 19.5. HRMS (ESI-FT-ICR) (*m*/*z*) [M + H]$^+$ calcd for 326.190326 (100%, $C_{24}H_{24}N$), found 326.190486 (100%, −0.5 ppm).

Compound 1. A mixture of **14** (323 mg, 1.2 mmol), 2,6-pyridinedicarboxylic acid chloride (102 mg, 0.5 mmol), and *N*,*N*-diisopropylethylamine (DIEA, 0.66 mL, 4 mmol) in dry CH_2Cl_2 (20 mL) was stirred under N_2 atmosphere overnight. The solution was concentrated under reduced pressure. The residue was purified by silica gel column chromatography (CH_2Cl_2/ethyl acetate = 200/1) to afford **1** as a white solid (187 mg, 56%). R_f = 0.7 (CH_2Cl_2/ethyl

DOI: 10.1021/acs.joc.5b01778
J. Org. Chem. 2015, 80, 11302−11312

acetate = 30/1). Mp > 300 °C. IR (KBr): 3410 (NH), 3062, 3022, 2925, 2856, 1695 (C═O), 1510, 1451, 1250, 991, 748, 624 cm^{-1}. ^1H NMR (400 MHz, $CDCl_3$), δ = 9.61 (s, 2H), 8.82 (d, 2H, J = 7.8 Hz), 8.37 (t, 1H, J = 7.8 Hz), 7.42−7.48 (m, 12H), 7.03−7.06 (m, 6H), 6.93−6.97 (m, 6H), 5.50 (s, 2H); ^{13}C NMR (100 MHz, $CDCl_3$), δ = 163.3, 149.8, 144.3, 142.5, 140.0, 126.7, 125.9, 125.1, 123.9, 120.9, 66.9, 53.8. HRMS (ESI-FT-ICR) (m/z) $[M + H]^+$ calcd for 670.2495 (100%, $^{12}C_{47}H_{32}N_3O_2$); 671.2528 ($^{12}C_{46}{}^{13}C_1H_{32}N_3O_2$); found 670.2509 (100%, 2.1 ppm), 671.2542 (60%, 2.1 ppm).

Compound 2. A mixture of 2,6-pyridinedicarboxylic acid (10.2 mg, 0.05 mmol), benzotriazol-1-yloxytripyrrolidinophosphonium hexafluorophosphate (PyBOP, 62.4 mg, 0.12 mmol), and 4-dimethylaminopyridine (DMAP, 24 mg, 0.2 mmol) in anhydrous DMF (20 mL) was stirred for 30 min. Then a solution of compound **16** (35 mg, 0.1 mmol) in anhydrous DMF was added, and the reaction mixture was refluxed under N_2 atmosphere for 2 days. The solution was concentrated under reduced pressure. Purification by silica gel column chromatography (CH_2Cl_2/ethyl acetate = 200/1) to afford **2** as a white solid (20 mg, 51%). R_f = 0.7 (CH_2Cl_2/ethyl acetate = 30/1). Mp > 300 °C. IR (KBr): 3412 (NH), 3075, 2925, 1701 (C═O), 1518, 1459, 1008, 849, 624 cm^{-1}. ^1H NMR (400 MHz, $CDCl_3$), δ = 9.86 (s, 2H), 8.77 (d, 2H, J = 7.6 Hz), 8.39 (t, 1H, J = 7.6 Hz), 7.12 (s, 6H), 7.06 (s, 6H), 5.18 (s, 2H), 2.03 (s, 18H), 1.59 (s, 18H); ^{13}C NMR (100 MHz, $CDCl_3$), δ = 163.2, 150.0, 142.4, 140.8, 140.3, 133.3, 132.7, 125.7, 124.9, 122.0, 66.0, 52.4, 19.4, 19.1. HRMS (ESI-FT-ICR) (m/z) $[M + H]^+$ calcd for 838.4373 (100%, $^{12}C_{59}H_{56}N_3O_2$); 839.4406 ($^{12}C_{58}{}^{13}C_1H_{56}N_3O_2$); found 838.4369 (100%, 0.0 ppm), 839.4467 (60%, 7.3 ppm).

Compound 3. Compound **3** was synthesized in a way similar to that described for **1** and obtained as a white solid in 52% yield. R_f = 0.7 (CH_2Cl_2/ethyl acetate = 30/1). Mp > 300 °C. IR (KBr): 3410 (NH), 3069, 2921, 1700 (C═O), 1518, 1459, 1383, 756, 619 cm^{-1}. ^1H NMR (400 MHz, acetone-d_6), δ = 9.97 (s, 2H), 8.67 (d, 2H, J = 7.2 Hz), 8.56 (t, 1H, J = 7.2 Hz), 7.49−7.55 (m, 8H), 7.24 (s, 1H), 7,15 (s, 1H), 7.03 (t, 4H, J = 7.2 Hz), 6.93 (t, 4H, J = 7.2 Hz), 5.61 (s, 2H), 2.01 (s, 6H), 1.32 (s, 6H); ^{13}C NMR (100 MHz, $CDCl_3$), δ = 163.4, 149.9, 144.5, 142.7, 142.1, 140.4, 140.3, 133.7, 133.2, 126.2, 125.8, 125.4, 125.1, 123.7, 121.6, 121.1, 66.6, 53.3, 19.4, 18.8. HRMS (ESI-FT-ICR) (m/z) $[M + H]^+$ calcd for 726.3121 (100%, $^{12}C_{51}H_{40}N_3O_2$); 727.3154 ($^{12}C_{50}{}^{13}C_1H_{56}N_3O_2$); found 726.3122 (100%, 0.1 ppm), 727.3209 (60%, 7.6 ppm).

Compound 4. Compound **4** was synthesized in a way similar to that described for **1** and obtained as a white solid in 47% yield. R_f = 0.7 (CH_2Cl_2/ethyl acetate = 30/1). Mp > 300 °C. IR (KBr): 3400 (NH), 3068, 3005, 2922, 2853, 1701 (C═O), 1519, 1459, 1384, 1263, 842, 754, 619 cm^{-1}. ^1H NMR (400 MHz, $CDCl_3$), δ = 9.82 (s, 2H), 8.76 (d, 2H, J = 8.0 Hz), 8.39 (t, 1H, J = 8.0 Hz), 7.36−7.42 (m, 4H), 7.15 (s, 4H), 7.03 (s, 4H), 6.91−7.01 (m, 4H), 5.27 (s, 2H), 2.02 (s, 12H), 1.26 (s, 12H); ^{13}C NMR (100 MHz, $CDCl_3$): δ = 163.3, 149.9, 144.6, 142.9, 142.2, 140.6, 140.4, 133.5, 132.9, 125.9, 125.7, 125.2, 124.9, 123.4, 121.8, 121.4, 66.3, 52.9, 19.4, 18.8. HRMS (ESI-FT-ICR) (m/z) $[M + H]^+$ calcd for 782.3747 (100%, $^{12}C_{55}H_{48}N_3O_2$); 783.3780 ($^{12}C_{54}{}^{13}C_1H_{48}N_3O_2$); found 782.3754 (100%, 0.9 ppm), 783.3779 (60%, −1.4 ppm).

■ ASSOCIATED CONTENT

Supporting Information

The Supporting Information is available free of charge on the ACS Publications website at DOI: 10.1021/acs.joc.5b01778.

CIF file of **1** cocrystallized with dichloromethane and methanol (CIF)
CIF file of **1** cocrystallized with acetonitrile (CIF)
CIF file of **1** cocrystallized with dichloromethane and methanol (CIF)
CIF file of **1** cocrystallized with acetonitrile (CIF)
CIF file of **1** cocrystallized with dichloromethane and methanol (CIF)
Video of rotational isomerization of **1** (AVI)
Video of rotational isomerization of **2** (AVI)
X-ray crystallographic data of **1**−**4**, VT NMR spectra and Eyring plot analyses of **1**−**4**, computational details, ^1H NMR, ^{13}C NMR, and 2D NMR spectra (PDF)

■ AUTHOR INFORMATION

Corresponding Authors

*E-mail: jiangh@bnu.edu.cn.
*E-mail: ywang1@bnu.edu.cn.
*E-mail: xuebochen@bnu.edu.cn.
*E-mail: ykche@iccas.ac.cn.

Notes

The authors declare no competing financial interest.

■ ACKNOWLEDGMENTS

We thank the National Natural Science Foundation of China (21125205 and 21332008) for financial support.

■ REFERENCES

(1) Sauvage, J.-P.; Amendola,V.; Ballardini, R.; Balzani, V.; Credi, A.; Fabbrizzi, L.; Gandolfi, M. T.; Gimzewski, J. K.; Gómez-Kaifer, M.; Joachim, C.; Kaifer, A. E.; Katz, E.; Kelly, T. R.; Liu, J.; Mangano, C.; Pallavicini, P.; Pease, A. R.; Raehm, L.; Sano, M.; Sauvage, J.-P.; Sestelo, J. P.; Shipway, A. N.; Stoddart, J.-F. ; Venturi, M.; Willner, I., Eds. *Molecular Machines and Motors*; Springer: Berlin, Germany, 2001.

(2) (a) Balzani, V.; Credi, A.; Raymo, F. M.; Stoddart, J. F. *Angew. Chem., Int. Ed.* **2000**, *39*, 3348−3391. (b) Kottas, G. S.; Clarke, L. I.; Horinek, D.; Michl, J. *Chem. Rev.* **2005**, *105*, 1281−1376. (c) Browne, W. R.; Feringa, B. L. *Nat. Nanotechnol.* **2006**, *1*, 25−35. (d) Kay, E. R.; Leigh, D. A.; Zerbetto, F. *Angew. Chem., Int. Ed.* **2007**, *46*, 72−191. (e) Michl, J.; Sykes, E. C. H. *ACS Nano* **2009**, *3*, 1042−1048.

(3) (a) Kao, C. Y.; Hsu, Y. T.; Lu, H. F.; Chao, I.; Huang, S. L.; Lin, Y. C.; Sun, W. T.; Yang, J. S. *J. Org. Chem.* **2011**, *76*, 5782−5792. (b) Chen, G.; Zhao, Y. *Org. Lett.* **2014**, *16*, 668−671.

(4) (a) Gan, Q.; Ferrand, Y.; Bao, C. Y.; Kauffmann, B.; Grélard, A.; Jiang, H.; Huc, I. *Science* **2011**, *331*, 1172−1175. (b) Blanco, V.; Leigh, D. A.; Marcos, V.; Morales-Serna, J. A.; Nussbaumer, A. L. *J. Am. Chem. Soc.* **2014**, *136*, 4905−4908.

(5) (a) Kelly, T. R.; et al. *J. Am. Chem. Soc.* **1994**, *116*, 3657−3658. (b) Nikitin, K.; Bothe, C.; Müller-Bunz, H.; Ortin, Y.; McGlinchey, M. J. *Organometallics* **2012**, *31*, 6183−6198.

(6) (a) Bedard, T. C.; Moore, J. S. *J. Am. Chem. Soc.* **1995**, *117*, 10662−10671. (b) Guenet, A.; Graf, E.; Kyritsakas, N.; Hosseini, M. W. *Inorg. Chem.* **2010**, *49*, 1872−1883. (c) Lang, T.; Graf, E.; Kyritsakas, N.; Hosseini, M. W. *Chem. - Eur. J.* **2012**, *18*, 10419−10426. (d) Zigon, N.; Larpent, P.; Jouaiti, A.; Kyritsakas, N.; Hosseini, M. W. *Chem. Commun.* **2014**, *50*, 5040−5042.

(7) Kelly, T. R. *Acc. Chem. Res.* **2001**, *34*, 514−522.

(8) (a) Kelly, T. R.; De Silva, H.; Silva, R. A. *Nature* **1999**, *401*, 150−152. (b) Koumura, N.; Zijlstra, R. W. J.; van Delden, R. A.; Harada, N.; Feringa, B. L. *Nature* **1999**, *401*, 152−155. (c) Fletcher, S. P.; Dumur, F.; Pollard, M. M.; Feringa, B. L. *Science* **2005**, *310*, 80−82. (d) Wang, J. B.; Feringa, B. L. *Science* **2011**, *331*, 1429−1432.

(9) Khuong, T. V.; Nunez, J. E.; Godinez, C. E.; Garcia-Garibay, M. A. *Acc. Chem. Res.* **2006**, *39*, 413−422.

(10) (a) Dominguez, Z.; Dang, H.; Strouse, M. J.; Garcia-Garibay, M. A. *J. Am. Chem. Soc.* **2002**, *124*, 2398−2399. (b) Nawara, A. J.; Shima, T.; Hampel, F.; Gladysz, J. A. *J. Am. Chem. Soc.* **2006**, *128*, 4962−4963. (c) Jarowski, P. D.; Houk, K. N.; Garcia-Garibay, M. A. *J. Am. Chem. Soc.* **2007**, *129*, 3110−3117. (d) Setaka, W.; Yamaguchi, K. *J. Am. Chem. Soc.* **2013**, *135*, 14560−14563. (e) Commins, P.; Garcia-Garibay, M. A. *J. Org. Chem.* **2014**, *79*, 1611−1619.

(11) (a) Hounshell, W. D.; Johnson, C. A.; Guenzi, A.; Cozzi, F.; Mislow, K. *Proc. Natl. Acad. Sci. U. S. A.* **1980**, *77*, 6961−6964. (b) Cozzi, F.; Guenzi, A.; Johnson, C. A.; Mislow, K.; Hounshell, W. D.; Blount, J. F. *J. Am. Chem. Soc.* **1981**, *103*, 957−958. (c) Johnson, C.

DOI: 10.1021/acs.joc.5b01778
J. Org. Chem. 2015, 80, 11302−11312

A.; Guenzi, A.; Mislow, K. *J. Am. Chem. Soc.* **1981**, *103*, 6240−6242. (d) Bürgi, H. B.; Hounshell, W. D.; Nachbar, R. B., Jr.; Mislow, K. *J. Am. Chem. Soc.* **1983**, *105*, 1427−1438.
(12) (a) Kawada, Y.; Iwamura, H. *J. Org. Chem.* **1980**, *45*, 2547−2548. (b) Kawada, Y.; Iwamura, H. *J. Am. Chem. Soc.* **1981**, *103*, 958−960. (c) Kawada, Y.; Iwamura, H. *Tetrahedron Lett.* **1981**, *22*, 1533−1536. (d) Iwamura, H.; Ito, T.; Ito, H.; Toriumi, K.; Kawada, Y.; Osawa, E.; Fujiyoshi, T.; Jaime, C. *J. Am. Chem. Soc.* **1984**, *106*, 4712−4717.
(13) (a) Johnson, C. A.; Guenzi, A.; Nachbar, R. B., Jr.; Blount, J. F.; Wennerstrom, O.; Mislow, K. *J. Am. Chem. Soc.* **1982**, *104*, 5163−5168. (b) Guenzi, A.; Johnson, C. A.; Cozzi, F.; Mislow, K. *J. Am. Chem. Soc.* **1983**, *105*, 1438−1448. (c) Kawada, Y.; Iwamura, H. *J. Am. Chem. Soc.* **1983**, *105*, 1449−1459.
(14) Kawada, Y.; Yamazaki, H.; Koga, G.; Murata, S.; Iwamura, H. *J. Org. Chem.* **1986**, *51*, 1472−1477.
(15) Iwamura, H.; Mislow, K. *Acc. Chem. Res.* **1988**, *21*, 175−182.
(16) (a) Koga, N.; Kawada, Y.; Iwamura, H. *J. Am. Chem. Soc.* **1983**, *105*, 5498−5499. (b) Koga, N.; Kawada, Y.; Iwamura, H. *Tetrahedron* **1986**, *42*, 1679−1686. (c) Chance, J. M.; Geiger, J. H.; Mislow, K. *J. Am. Chem. Soc.* **1989**, *111*, 2326−2327. (d) Chance, J. M.; Geiger, J. H.; Okamoto, Y.; Aburatani, R.; Mislow, K. *J. Am. Chem. Soc.* **1990**, *112*, 3540−3547.
(17) Kawada, Y.; Sakai, H.; Oguri, M.; Koga, G. *Tetrahedron Lett.* **1994**, *35*, 139−142.
(18) Setaka, W.; Nirengi, T.; Kabuto, C.; Kira, M. *J. Am. Chem. Soc.* **2008**, *130*, 15762−15763.
(19) Frantz, D. K.; Baldridge, K. K.; Siegel, J. S. *Chimia* **2009**, *63*, 201−204.
(20) Frantz, D. K.; Linden, A.; Baldridge, K. K.; Siegel, J. S. *J. Am. Chem. Soc.* **2012**, *134*, 1528−1535.
(21) Bryan, J. C.; Sachleben, R. A.; Gakh, A. A.; Bunick, G. J. *J. Chem. Crystallogr.* **1999**, *29*, 513−521.
(22) (a) Dolain, C.; Maurizot, V.; Huc, I. *Angew. Chem., Int. Ed.* **2003**, *42*, 2738−2740. (b) Haldar, D.; Jiang, H.; Léger, J. M.; Huc, I. *Tetrahedron* **2007**, *63*, 6322−6330. (c) Monchaud, D.; Yang, P.; Lacroix, L.; Teulade-Fichou, M. P.; Mergny, J. *Angew. Chem., Int. Ed.* **2008**, *47*, 4858−4861.
(23) Morse, J. K. *Proc. Natl. Acad. Sci. U. S. A.* **1927**, *13*, 789−793.
(24) Stevens, A. M.; Richards, C. J. *Tetrahedron Lett.* **1997**, *38*, 7805−7808.
(25) (a) Friedman, L.; Logullo, F. M. *J. Org. Chem.* **1969**, *34*, 3089−3092. (b) Klanderman, B. H.; Criswell, T. R. *J. Org. Chem.* **1969**, *34*, 3426−3430.
(26) (a) Yamamoto, G.; Higuchi, H.; Yonebayashi, M.; Nabeta, Y.; Ojima, J. *Tetrahedron* **1996**, *52*, 12409−12420. (b) Yamamoto, G.; Agawa, C.; Ohno, T.; Minoura, M.; Mazaki, Y. *Bull. Chem. Soc. Jpn.* **2003**, *76*, 1801−1811.
(27) Theilacker, W.; Beyer, K.-H. *Chem. Ber.* **1961**, *94*, 2968−2977.
(28) Sala, M.; Kirkby, O. M.; Guérin, S.; Fielding, H. H. *Phys. Chem. Chem. Phys.* **2014**, *16*, 3122−3133.
(29) Bobadova-Parvanova, P.; Jackson, K. A.; Srinivas, S.; Horoi, M.; KÖhler, C.; Seifert, G. *J. Chem. Phys.* **2002**, *116*, 3576−3587.
(30) Frisch, M. J.; Trucks, G. W.; Schlegel, H. B.; Scuseria, G. E.; Robb, M. A.; Cheeseman, J. R.; Montgomery, J. A., Jr.; Vreven, T.; Kudin, K. N.; Burant, J. C.; Millam, J. M.; Iyengar, S. S.; Tomasi, J.; Barone, V.; Mennucci, B.; Cossi, M.; Scalmani, G.; Rega, N.; Petersson, G. A.; Nakatsuji, H.; Hada, M.; Ehara, M.; Toyota, K.; Fukuda, R.; Hasegawa, J.; Ishida, M.; Nakajima, T.; Honda, Y.; Kitao, O.; Nakai, H.; Klene, M.; Li, X.; Knox, J. E.; Hratchian, H. P.; Cross, J. B.; Adamo, C.; Jaramillo, J.; Gomperts, R.; Stratmann, R. E.; Yazyev, O.; Austin, A. J.; Cammi, R.; Pomelli, C.; Ochterski, J. W.; Ayala, P. Y.; Morokuma, K.; Voth, G. A.; Salvador, P.; Dannenberg, J. J.; Zakrzewski, V. G.; Dapprich, S.; Daniels, A. D.; Strain, M. C.; Farkas, O.; Malick, D. K.; Rabuck, A. D.; Raghavachari, K.; Foresman, J. B.; Ortiz, J. V.; Cui, Q.; Baboul, A. G.; Clifford, S.; Cioslowski, J.; Stefanov, B. B.; Liu, G.; Liashenko, A.; Piskorz, P.; Komaromi, I.; Martin, R. L.; Fox, D. J.; Keith, T.; Al-Laham, M. A.; Peng, C. Y.; Nanayakkara, A.; Challacombe, M.; Gill, P. M. W.; Johnson, B.; Chen, W.; Wong, M. W.; González, C.; Pople, J. A. Gaussian03 Revision D.02; Gaussian, Inc.: Pittsburgh, PA, 2004.
(31) (a) Roussel, C.; Vanthuyne, N.; Bouchekara, M.; Djafri, A.; Elguero, J.; Alkorta, I. *J. Org. Chem.* **2008**, *73*, 403−411. (b) Dial, B. E.; Pellechia, P. J.; Smith, M. D.; Shimizu, K. D. *J. Am. Chem. Soc.* **2012**, *134*, 3675−3678.
(32) (a) Zhang, Z. Y.; Wu, Y. S.; Tang, K. C.; Chen, C. L.; Ho, J. W.; Su, J. H.; Tian, H.; Chou, P. T. *J. Am. Chem. Soc.* **2015**, *137*, 8509−8520. (b) Huang, W.; Sun, L.; Zheng, Z. W.; Su, J. H.; Tian, H. *Chem. Commun.* **2015**, *51*, 4462−4464.
(33) Rohonczy, J. *DNMR Line Shape Analysis*, Software Manual, version 1.1; Bruker BioSpin GmbH: Rheinstetten, 2007.
(34) For examples studies that use VT ^{13}C NMR to avoid the analysis of complicated VT ^{1}H NMR spectra for thermodynamic parameters, see: (a) Yang, J. S.; Huang, Y. H.; Ho, J. H.; Sun, W. T.; Huang, H. H.; Lin, Y. C.; Huang, S. J.; Huang, S. L.; Lu, H. F.; Chao, I. *Org. Lett.* **2008**, *10*, 2279−2282. (b) Sun, W. T.; Huang, Y. T.; Huang, G. J.; Lu, H. F.; Chao, I.; Huang, S. L.; Huang, S. J.; Lin, Y. C.; Ho, J. H.; Yang, J. S. *Chem. - Eur. J.* **2010**, *16*, 11594−11604. (c) Sun, W. T.; Huang, S. L.; Yao, H. H.; Chen, I. C.; Lin, Y. C.; Yang, J. S. *Org. Lett.* **2012**, *14*, 4154−4157.
(35) The free energy of activation ($\Delta G^{\ddagger}$), the enthalpy ($\Delta H^{\ddagger}$), and the entropy ($\Delta S^{\ddagger}$) were derived from the Eyring plots. See (a) Sandstrom, J. *Dynamic NMR Spectroscopy*; Academic Press: London, 1982. (b) Zimmer, K. D.; Shoemaker, R.; Ruminski, R. R. *Inorg. Chim. Acta* **2006**, *359*, 1478−1484.
(36) A similar phenomenon has been also observed in other molecular rotary systems. For example, see Chen, Y. C.; Sun, W. T.; Lu, H. F.; Chao, I.; Huang, G. J.; Lin, Y. C.; Huang, S. L.; Huang, H. H.; Lin, Y. D.; Yang, J. S. *Chem. - Eur. J.* **2011**, *17*, 1193−1200.
(37) 2,3,6,7-Tetramethylanthracene was synthesized according to the procedures reported in the following literature: (a) Hess, H. J.; Cronin, T. H.; Scriabine, A. *J. Med. Chem.* **1968**, *11*, 130−136. (b) Bender, D.; Mullen, K. *Chem. Ber.* **1988**, *121*, 1187−1197. (c) Godinez, C. E.; Zepeda, G.; Mortko, C. J.; Dang, H.; Garcia-Garibay, M. A. *J. Org. Chem.* **2004**, *69*, 1652−1662.
(38) Zhu, X. Z.; Chen, C. F. *J. Am. Chem. Soc.* **2005**, *127*, 13158−13159.
(39) Compound **8** was obtained according to the procedure reported in ref 25b, and the compound was used directly without further purification.

DOI: 10.1021/acs.joc.5b01778
J. Org. Chem. 2015, 80, 11302−11312